



Localization of cavities in cast components via impulse excitation and a finite element analysis

Philipp Lechner¹ · Erwin Reberger¹ · Maximilian Gruber¹ · Simon Kammerloher¹ · Christoph Hartmann¹ · Wolfram Volk¹

Received: 29 October 2021 / Accepted: 4 May 2022 / Published online: 4 June 2022
© The Author(s) 2022

Abstract

In this work, the acoustic resonance testing method has been extended by a finite element analysis of the examined component to localize cavities within die casting parts. This novel method aims at a fast and efficient quality inspection which allows hidden cavities in cast components to be detected, which is only possible with X-ray technology at the moment. The promising results show that this method enables the localization of shrinkage cavities. Furthermore, the influence of product scatter has been analyzed regarding the accuracy of the calculated position of artificial defects.

Keywords Quality inspection · Die casting · Acoustic resonance testing · Impulse excitation · Casting defects

1 Introduction

Quality assurance is a key aspect of modern mass production in general and of casting processes in particular. Compared to other mass production techniques like metal forming and machining, metal casting has a comparatively high percentage of scrap parts with defects. Due to complex process control, casting defects like cavities occur in the components, which have to be detected in a quality assurance process. Depending on the geometry of the part and the casting process itself, these cavities cannot be detected by visual inspection, since they are not visible on the surface. Therefore, quality assurance methods have to analyze the whole volume of the component for defects.

1.1 Acoustic resonance testing

Acoustic resonance testing (ART) as a nondestructive testing method is based on the excitation of a specimen by an external mechanical impulse [1]. Hitting the specimen with a hammer is a suitable method for impulse excitation [2]. Alternative excitement methods are for example a ball

drop, dropping the specimen, laser pulses, or compressed air pulses [1]. Ideally, this impulse provides constant energy at all frequencies which causes the specimen to vibrate in its inherent eigenmodes and corresponding eigenfrequencies [3]. This vibration is long-lasting since resonance within the specimen is obtained. Other frequencies which do not correspond to the excited eigenmodes—thus are not resonant—die out quickly [4]. Damping leads to a slowly decreasing vibration of resonant modes that eventually die out with time, due to inner friction of the specimen.

The occurring eigenmodes, eigenfrequencies and damping factors represent the vibration characteristics of the specimen. A physical signal results from measurement with a microphone, laser vibrometer or accelerometer [1]. Deviations and flaws influence the vibration characteristics of a specimen which is exploited for qualitative comparison [5]. Thus, ART compares the measured physical signal of the examined specimen against a reference signal of already sampled specimens which are within component specifications (OK part). There are already first studies which analyze the possibility of locating flaws in components based on simulation data. Lai et al. found it possible to locate flaws from a theoretical point of view and that the effects of multiple flaws can be simplified by linear superposition [6]. Furthermore, Lai and Sun found that changes to the eigenfrequencies of a component due to varying physical properties, like density, can be calculated with a linear regression model [7]. This research group also analyzed the

✉ Philipp Lechner
philipp.lechner@utg.de

¹ Chair of Metal Forming and Casting, Technical University of Munich, Walther-Meissner-Str. 4, 85748 Garching, Germany

influence of the defect type (cavity, crack, mixed) on the location of a flaw based on simulation data [8]. Schmidt and Steinbuch analyzed the effect of mechanical flaws in components in comparison to manufacturing tolerances [9, 10]. They found that the flaw location significantly correlates with specific eigenmodes. This allows to pinpoint the flaw to areas in the component which influence the eigenmode most. Zhang and Yan combined a systematic FEM approach with experimental measurements and showed that it is possible to locate multiple cracks in a simple cantilever geometry [11].

1.2 Quality assurance of cast parts

Almost all cast components have shrinkage cavities of different sizes, starting with micro pores [12]. If a cast component is scrap (NOK) or an OK part, depends on the size of the cavities, their position and the quality specifications of the component [13]. Therefore, it is important that methods for quality inspection are able to localize cavities, since the presence of a cavity might be tolerable in one area of the component, while it is not in another. X-ray tomography is the standard method for scanning cast parts for defects, since it is able to determine the position and size of cavities with high accuracy [14]. However, the process of X-ray tomography is very time-consuming and expensive. In recent years the interpretation of the X-ray images has been automated with artificial intelligence for some use cases [15]. Nevertheless, industry standard is still the analysis of the images by skilled workers.

Therefore, some articles have proposed to implement acoustic resonance testing as a low cost alternative [16]. Psiuk et al. utilize the impulse excitation method for monitoring a gel casting process of ceramics [17]. However, these methods are only able to detect an acoustic difference between an ideal part and the specimen in question. It is not possible to further investigate the cause for a discrepancy in the frequency domain, which would lead to more information about the defect [16].

This article aims to overcome these issues and studies whether it is possible to experimentally localize cavities in die casting components via impulse excitation technique. Furthermore, it analyzes how the position of the cavity and the tolerances of the components, which are determined by the die casting process, affect this localization.

2 Materials and methods

2.1 Specimens

The specimens utilized for this article are aluminum angle brackets, produced with a high pressure die casting process. The chemical composition of the alloy has been determined with an Optical Emission Spectrometer Foundry-Master from Worldwide Analytical Systems GmbH and is presented in Table 1. The chemical composition corresponds well to the aluminum alloy EN 46100, which is a typical die casting alloy [18]. The elastic modulus was determined with a “Nanotest Vantage” (Micro Materials Limited), equipped with a spherical tip according to the method of Oliver & Pharr [19] and the measurement procedure described by Lechner et al. [20]. One specimen was tested in 75 locations which led to a reduced modulus of 97.4 GPa with a standard deviation of 7.14 GPa. With a Poisson ratio of 0.33 this leads to an elastic modulus of 93.7 GPa.

50 unmodified pieces have been analyzed with impulse excitation to quantify scatter for each natural frequency resulting from product tolerances due to the die casting process. Furthermore, holes have been added to three angle brackets to emulate casting defects. The position of the cavities is varied for a parameter study. The bracket angle is shown in Fig. 1 with the positions of the holes P1–P3. For each position one bracket angle was adapted with a hole of 5 mm diameter.

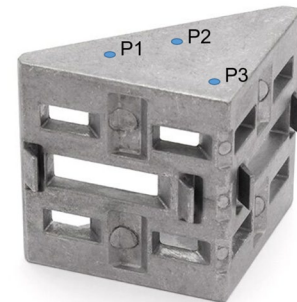


Fig. 1 Specimen utilized in this article. On the top side, three positions P1–P3 are marked as blue circles, where holes are drilled into the specimens as artificial casting defects

Table 1 Chemical composition of the utilized specimens

Al	Si	Fe	Cu	Mn
84.0	12.1	0.825	1.87	0.162
Mg	Cr	Ni	Zn	Ti
0.159	0.0433	0.143	0.498	0.0459

2.2 Test bench

The main component is a horizontal frame, that supports a portal frame and a rotatory table (Physik Instrumente, M-037) which is driven by a stepper motor. Overall, the test bench has dimensions of approximately 470 mm × 470 mm × 380 mm and is depicted in Fig. 2.

The specimens are positioned on relocatable conical rubber buffers on a turntable subdivided into five segments. It is mounted to the rotatory table and allows for five tests within a test cycle. This concept ensures flexibility in positioning and approximately free vibration of the specimens.

A solenoid is used for impulse excitation. It is mounted to the portal frame, which is adjustable in all directions in space. Consequently, the solenoid can be positioned to avoid multiple or long-lasting contact with the specimen. Its stroke is 25 mm and the holding force at the end of the stroke is up to 45 N. The hammer of the solenoid is lightweight, which has several advantages. First, it accelerates quickly. Second, it reflects well from the surface of the specimen, which helps to avoid double contacts and long contact times. Furthermore, the microphone is mounted to the portal frame next to the solenoid. We performed preliminary experiments regarding the position of the microphone and found that it is advantageous if the microphone is positioned approximately 15 mm from the analyzed component, but has as much distance to the location of impact as possible to reduce the noise of the solenoid in the signal.

A single-board computer (Raspberry Pi 3 B+) controls the test routine of the test bench. It communicates via serial connections with a microcontroller (Arduino UNO Rev3)

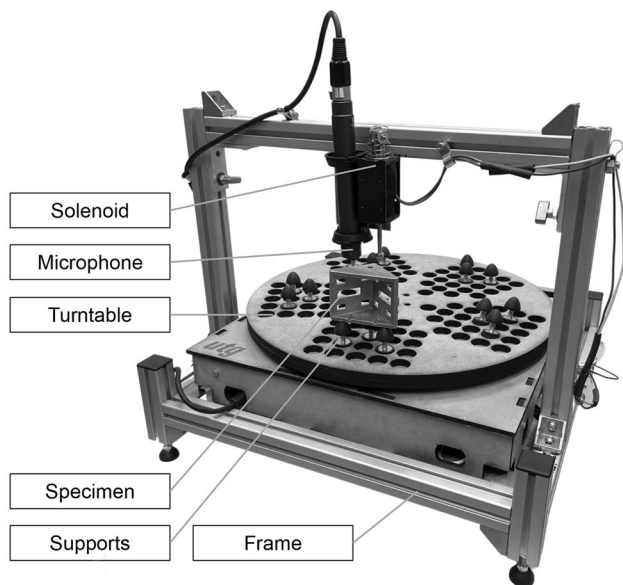


Fig. 2 Test bench for Acoustic Resonance Testing

and a control unit to which the microphone is connected. The microcontroller drives both the stepper motor and the solenoid. Furthermore, it reads the signal of the microswitch, which is used for homing the rotatory table. The test routine is implemented via a custom python program on the Raspberry Pi. The program builds on the library PyQt5; Within the test routine, all necessary processes for operating the test bench are invoked. This includes bilateral communication to the Arduino board in order to actuate the mechatronic components. Also, the recording process, data processing and data visualization are handled by the program.

2.3 Modal analysis and spatial sensitivity

The modal analysis in this article has been performed in Abaqus 2018 with the Finite Element Method (FEM). A geometrical model of the specimens was meshed with tetrahedron C3D10 [21] quadratic elements and a seed distance of 2 mm. The calculation was performed with a Lanczos solver up to 20 kHz. The meshed model is shown in Fig. 3, with a 5 mm hole (top) and without a cavity (bottom). The coordinate system which will be utilized in the following is depicted in Fig. 3, as well. The artificial cavity can be moved systematically through the component with a python script. The model has two symmetry planes and the one which is

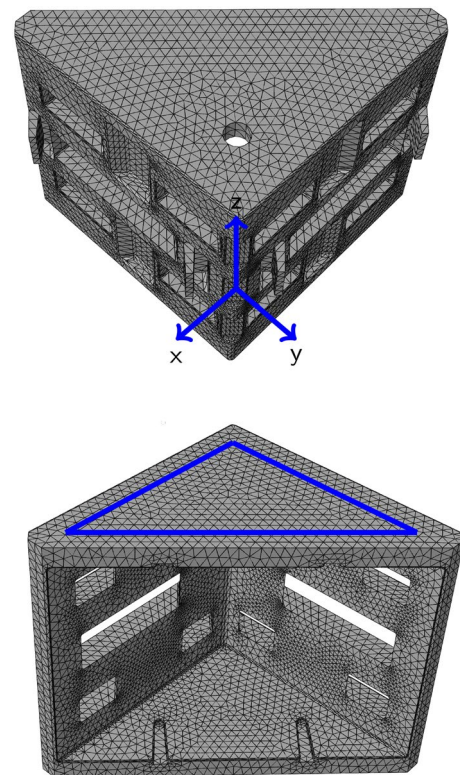


Fig. 3 FE model meshed with 2 mm tetrahedron elements. The drilled hole can be systematically moved through the component (top)

defined by the z-axis and the points P2 and P3 affects this study. Therefore, we expect identical results in the marked triangle in Fig. 3 for positions which are symmetrical to the P2–P3 axis. To avoid edge effects, the hole is only moved in the blue area of Fig. 3 (bottom), which has a minimum distance from the borders of the top surface of 3 mm. Therefore, open holes are avoided for this feasibility study. The material model for the FE simulation is purely elastic with a density of 2700 kg/m³ [18].

In a first step, it is necessary to analyze how the position of a cavity in the cast part affects the eigenfrequencies of the specimens. Therefore, a hole with 5 mm diameter was moved systematically in the simulation model in the area specified in Fig. 3. The eigenfrequencies of the model are calculated for a regular hole grid of 2 mm distance and interpolated between those grid points. These results are compared to the calculated eigenfrequencies of a bracket angle without a cavity and normalized. This change is calculated as follows:

$$\Delta f_i = \frac{f_i^{sim} - g_i^{sim}(x, y)}{f_i^{sim}} \quad (1)$$

The results are detailed in Sect. 3.1.

2.4 Test procedure

To test the feasibility of a cavity localization, three specimens with 5 mm holes in different locations P1–P3 are analyzed on the test bench from Sect. 2.2. The results are compared to an average spectrum of ten randomly chosen specimens without a cavity to emulate realistic conditions for an industrial application. The comparison of the resonance spectrum of one specific specimen prior and post drilling seems too trivial. When comparing one specimen to a representative sample size, the experiment serves as a first indicator how the characterization method copes with product scatter, which affects the resonance spectrum. The results of this study are presented in Sect. 3.2.

Furthermore, the eigenfrequencies of the three specimens with holes at the positions P1–P3 are compared to 40 specimens without a cavity to predict the position of the cavity. These results allow to analyze the influence of the manufacturing tolerances on the accuracy of the measurement, which will be presented in the second part of Sect. 3.2.

2.5 Algorithm to locate the cavity

Preliminary experiments have shown that the eigenfrequencies 1–13 can be detected automatically in the experimental signal. Therefore, these frequencies are utilized for this

analysis. The average spectrum ensures that the test conditions for the algorithm are representative for an industrial application. The eigenfrequencies of the average specimen are denoted with f_i , while the eigenfrequencies of the specimen with a cavity are denoted g_i , where i is the number of a specific eigenmode. Expression 2 describes the term which is minimized with respect to the variables x and y being the coordinates of the flaw. The minimum root mean square error for all eigenfrequencies yields the predicted position of the flaw.

In expression 2, the relative effects of a cavity in the simulation are compared to the effects of a cavity in the experimental specimens. The minimum with respect to all 13 eigenfrequencies leads to the prediction of the cavity position. Each eigenfrequency is normalized with the first eigenfrequency in the corresponding spectrum. This reduces the influence of fluctuating stiffness in the specimens' population. Ideally, the simulation models the geometry and the material of each part accurately. However, inaccuracies of the simulation model compared to each specimen result from production tolerances which are typical for die cast parts, for example variations of the geometry and the elastic constants. Both depend strongly on the current process conditions which can vary from part to part. Therefore, a fault tolerant formulation of the minimization problem is necessary. This relative comparison is advantageous since inaccuracies in the simulation model can be disregarded as long as the relative effect of the cavity is not affected. The symmetry in the specimen has been utilized to reduce the calculation effort.

$$\min(x, y) \left\{ \left[\sum_{i=1}^{13} \left(\frac{f_i^{exp}/f_1^{exp} - g_i^{exp}/g_1^{exp}}{f_i^{exp}/f_1^{exp}} - \frac{f_i^{sim}/f_1^{sim} - g_i^{sim}(x, y)/g_1^{sim}(x, y)}{f_i^{sim}/f_1^{sim}} \right)^2 \right]^{\frac{1}{2}} \right\} \quad (2)$$

Furthermore, a compensation for varying physical properties of the specimens is utilized to improve the prediction results and to cope with the manufacturing tolerances. The mass is determined and utilized to adapt the measured eigenfrequencies with a linear regression model analogous to the calculation proposed by Lai and Sun [7], who found that a linear function is able to describe the influence of a change in density of up to 3%. Therefore, a factor is calculated for each eigenfrequency with a best fit to describe the linear function between the mass and each eigenfrequency. These factors are utilized to correct the deviation from the mean of the mass, which is implemented in the finite element simulation.

3 Results and discussion

3.1 Spatial sensitivity analysis

The results of the spatial sensitivity analysis are depicted in Fig. 4 for eigenfrequencies 1–8. The color of every pixel indicates the change of the respective eigenfrequency if a hole of 5 mm diameter is added to this position. Figure 4 shows the important result that cavities in certain areas of the bracket angle influence the eigenfrequencies in a specific manner, which hopefully allows the cavity to be located by comparing this specific combination of eigenfrequencies to a specimen without a cavity. Furthermore, the results are symmetrical to the symmetry plane of the angle bracket, which is not surprising. Therefore, it is not possible to differentiate between two symmetrical locations. However, from a technical point of view, this seems not problematic. The reason for the localization of cavities is the evaluation, if the component is scrap or within specifications. Typically, technical specifications do not differentiate between symmetric areas of a component, either. Therefore, the technical goal for this study is not affected. The results of the section lead to the conclusion, that a localization of the cavity is possible in principle, which will be studied in the next section.

3.2 Flaw localization and influence of manufacturing tolerances

The results for the estimation of hole positions P1–P3 are shown in Fig. 5. The predicted position of the cavity is depicted in blue, while the flaw is depicted in red. The systematic error is 4.5 mm for P1, 3.2 mm for P2 and 2.8 mm for P3. Repeating the determination of the eigenfrequencies for a specimen nine times showed that the random measuring error is negligible. For repeated measurements, the mean standard deviation for all recorded eigenfrequencies is 0.007 %, which does not alter the predicted cavity position.

These first experiments show, that it is possible to estimate the position of the cavity by utilizing expression 2 and comparing the spectrum of one specimen to the mean spectrum of ten specimens. The remaining systematic error results from model errors, which are deviations of the material properties density and Young's modulus and deviations of the geometry. Homogeneous fluctuations of the Young's modulus or the density which change the eigenfrequencies by a constant factor are negligible due to the normalization and the relative calculation of the global minimum in expression 2. Therefore, the systematic error results from inhomogeneous scatter of these properties. For example, the solidification in the die casting process can vary locally due to scatter in the coating thickness of the mold, which locally influences the Young's modulus. The next step will analyze

the extent of this scatter from part to part and its influence on the estimation of the cavity position.

To quantify the systematic error, 40 specimens have been compared individually to each of the specimens with a hole in positions P1–P3. This leads to a mean systematic error of 7.9 mm for P1, 3.7 mm for P2 and 3.1 mm for P3. The standard deviations are 4.1 mm, 3.9 mm and 1.9 mm (P1–P3), if expression 2 is utilized without further information about the specimens. Additionally, the mass of the specimen was utilized to adapt the measured eigenfrequencies, as described in Sect. 2.5. This leads to an improvement of the systematic error and the corresponding standard deviations. The results are detailed in Table 2

Figure 6 depicts a scatter plot with the predicted centers of each flaw marked with blue dots after the implementation of the regression model. For each flaw position P1–P3, the individual predictions are grouped around the flaws. The mean systematic error is 7.9 mm for P1, 3.0 mm for P2 and 2.8 mm for P3. The standard deviations are 2.6 mm, 1.9 mm and 1.8 mm. These results show that the systematic error and the scatter depend significantly on the position in the component. Therefore, the local manufacturing tolerances should be analyzed in the future to further quantify the spatial accuracy of this method.

4 Discussion of industrial applicability and remaining future work

From an industrial application point of view, these are promising first results. Combined with an FEM modal analysis it may be possible in the future to not only detect cavities in complex industrial components, but also to localize them in specific areas of the component. At the moment, this is already possible for the specimens at hand for single flaws with a constant flaw size. The accuracy of the localization depends on the position of the flaw in the component and product scatter due to the casting process. With the algorithm at hand it is possible to inspect cast parts and to automatically compute an evaluation if the component is within specifications or not in only a few seconds compared to a much longer time and effort in X-ray tomography. Thus, there is still remaining research work to do to reach industrial applicability. In future work, we will characterize in detail the product scatter for exemplary cast parts. This allows a monte carlo analysis of the inspection process which leads to a quantitative probabilistic estimation of flaw positions in cast components. Therefore, the inspection results can be expressed as a probability of an OK part. Furthermore, the influence of multiple flaws and their respective size has to be investigated.

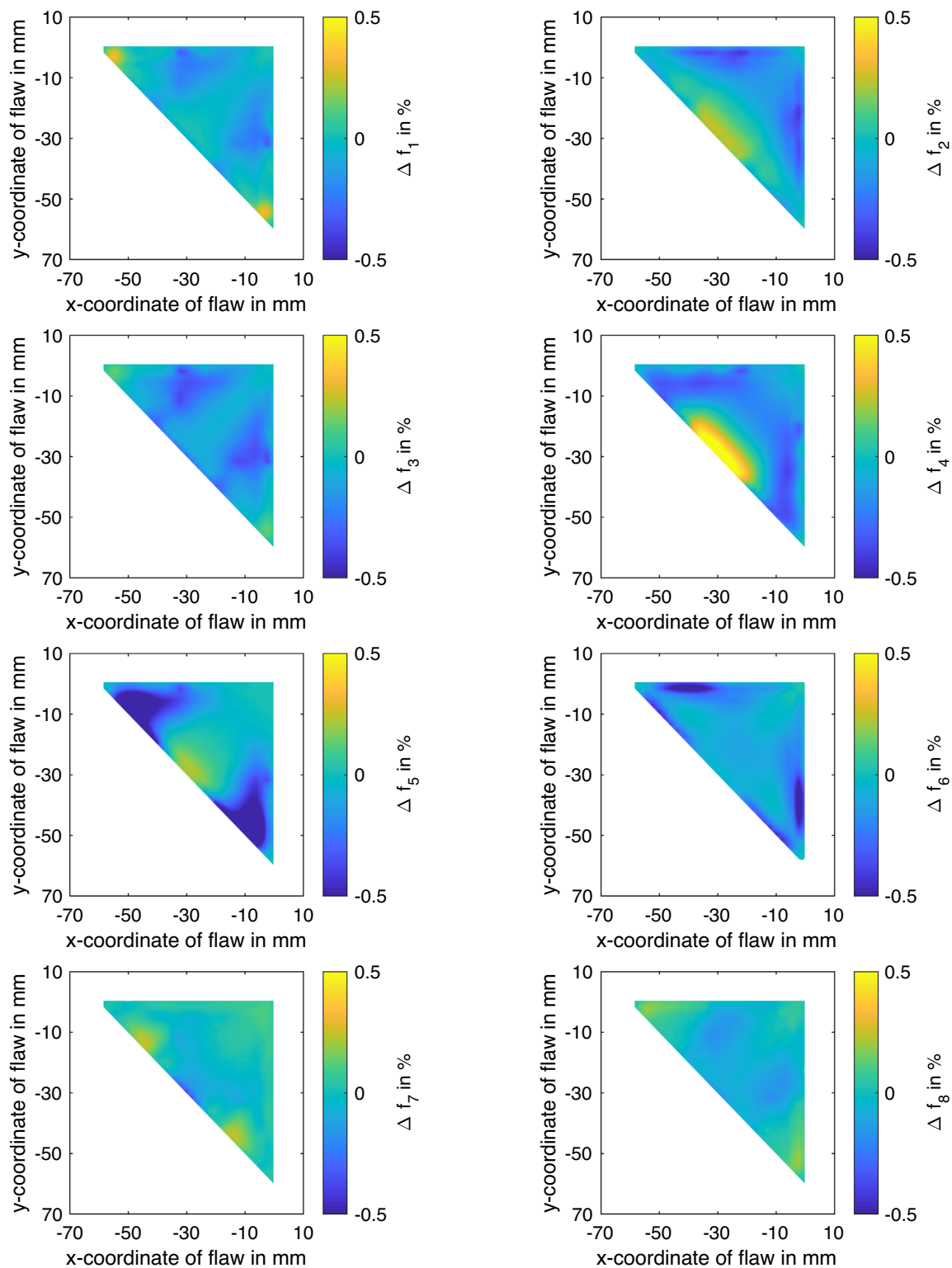


Fig. 4 Spatial sensitivity analysis for the first eight eigenmodes. The color of every pixel indicates the change to the respective eigenfrequency if a hole of 5 mm diameter is added to this position

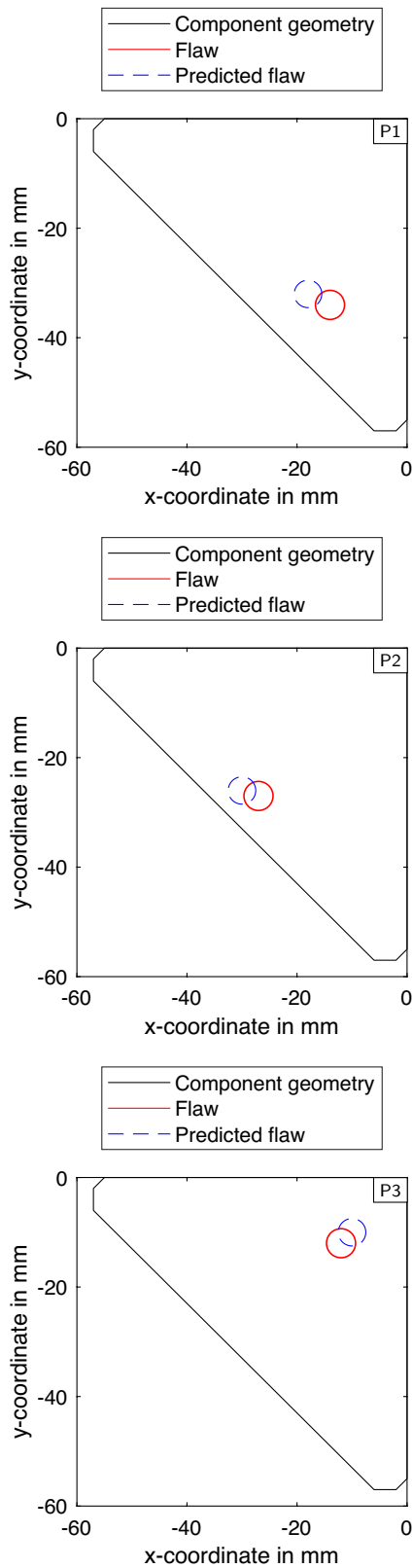


Fig. 5 Results of a cavity localization with expression 2 for positions P1–P3. The predicted position of the cavity is depicted in dashed blue, while the flaw is depicted in solid red

Table 2 Mean systematic error and standard deviation (Std) of the estimation of the cavity position without additional data and with the linear regression incorporating mass of the specimens

	P1 (mm)	P2 (mm)	P3 (mm)
Equation 2	7.9	3.7	3.1
Std	4.1	3.9	1.9
Equation 2 with regression	7.9	3.0	2.8
Std	2.6	1.9	1.8

5 Conclusion

In this article, we studied the feasibility of a flaw localization in die cast parts by applying acoustic resonance testing combined with a finite element analysis of the cast component. The presented results show that it is possible to locate a flaw in a specific area of the specimen. A degree of uncertainty will remain after the acoustic assessment. However, this will lead to quality improvement for a lot of casting products which are currently not checked for cavities at all, for cost reasons. These first results are promising that a fast and efficient quality inspection method is possible, which has significantly lower cost per part than X-ray tomography.

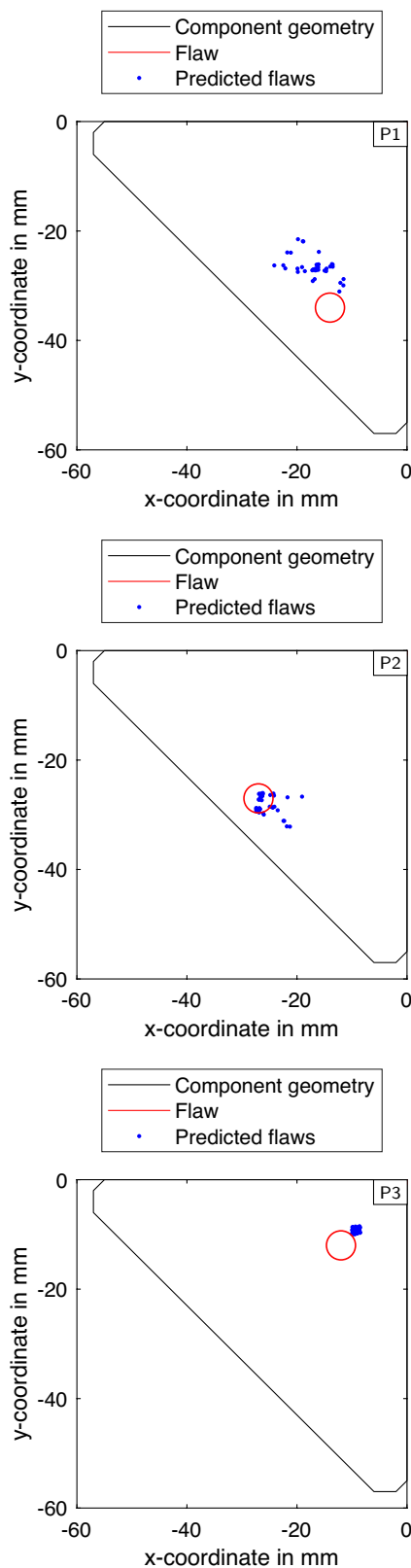


Fig. 6 Scatter plot of flaw predictions

Acknowledgements The authors thank Maria Schmuck for her support in characterizing the specimens.

Funding Open Access funding enabled and organized by Projekt DEAL. Funded by the Deutsche Forschungsgemeinschaft (DFG, German Research Foundation), project numbers: 374548845, 445163571 and 407354049.

Declarations

Conflicts of interest The authors have no conflicts of interest to declare that are relevant to the content of this article.

Open Access This article is licensed under a Creative Commons Attribution 4.0 International License, which permits use, sharing, adaptation, distribution and reproduction in any medium or format, as long as you give appropriate credit to the original author(s) and the source, provide a link to the Creative Commons licence, and indicate if changes were made. The images or other third party material in this article are included in the article's Creative Commons licence, unless indicated otherwise in a credit line to the material. If material is not included in the article's Creative Commons licence and your intended use is not permitted by statutory regulation or exceeds the permitted use, you will need to obtain permission directly from the copyright holder. To view a copy of this licence, visit <http://creativecommons.org/licenses/by/4.0/>.

References

- Weidner M (2017) Qualitätsprüfung seriengefertigter bauteile mit akustischer resonanzanalyse. *Giesserei-Praxis* 06:240–243
- Lechner P, Fuchs G, Hartmann C, Steinlehner F, Etmeyer F, Volk W (2020) Acoustical and optical determination of mechanical properties of inorganically-bound foundry core materials. *MDPI Mater* 13:2531
- Sankaran V (2011) Low cost inline ndt system for internal defect detection in automotive components using acoustic resonance testing. In: *Proceedings of the National Seminar & Exhibition on Non-Destructive Evaluation*, pp 237–239
- Coffey E (2012) Acoustic resonance testing. In: *Future of Instrumentation International Workshop (FIIW)*. *Proceedings*, pp 1–2
- Heinrich M, Rabe U (2020) Simulation-based generation of representative and valid training data for acoustic resonance testing. *MDPI Appl Sci* 10:6059
- Lai C, Xu W, Sun X (2012) Predicting flaw-induced resonance spectrum shift with theoretical perturbation analysis. *J Vib Acoust*. <https://doi.org/10.1115/1.4006649>
- Xu W, Lai C, Sun X (2015) Identify structural flaw location and type with an inverse algorithm of resonance inspection. *J Vib Control* 21(13):2685. <https://doi.org/10.1177/1077546313516823>
- Xu W, Lai C, Sun X (2015) *J Vib Control* 21(13):2685. <https://doi.org/10.1177/1077546313516823>
- Schmidt L, Steinbuch R (2002) Improved interpretation of the acoustic response spectrum to identify types of component deviations. *Res Nondestr Eval* 14(2):95. <https://doi.org/10.1080/09349840209409707>
- Steinbuch R (2005) Scatter or defect? some remarks on the interpretation of acoustic spectral shift. *Res Nondestr Eval* 15(4):173. <https://doi.org/10.1080/09349840490915645>

11. Zhang K, Yan X (2017) Multi-cracks identification method for cantilever beam structure with variable cross-sections based on measured natural frequency changes. *J Sound Vib* 387:53. <https://doi.org/10.1016/j.jsv.2016.09.028>. <https://www.sciencedirect.com/science/article/pii/S0022460X16304953>
12. Nicoletto G, Konečná R, Fintova S (2012) Characterization of microshrinkage casting defects of al–si alloys by x-ray computed tomography and metallography. *Int J Fatigue* 41(3):39. <https://doi.org/10.1016/j.ijfatigue.2012.01.006>
13. Vijayaram TR, Sulaiman S, Hamouda A, Ahmad M (2006) Foundry quality control aspects and prospects to reduce scrap rework and rejection in metal casting manufacturing industries. *J Mater Process Technol* 178(1–3):39. <https://doi.org/10.1016/j.jmatprotec.2005.09.027>
14. Noble A, Hartley R, Mundy J, Farley J (1994) X-ray metrology for quality assurance. In: *Proceedings of the IEEE International Conference on robotics and automation (IEEE Comput. Soc. Press, 1994)*, pp. 1113–1119. <https://doi.org/10.1109/ROBOT.1994.351211>
15. Du W, Shen H, Fu J, Zhang G, He Q (2019) Approaches for improvement of the x-ray image defect detection of automobile casting aluminum parts based on deep learning. *NDT & E Int* 107:102144. <https://doi.org/10.1016/j.ndteint.2019.102144>
16. Białobrzeski A (2013) An attempt to use sonic testing in casting quality assessment. *Adv Manuf Sci Technol* 37(1):10. <https://doi.org/10.2478/amst-2013-0008>
17. Psiuk B, Wieceńska P, Lipowska B, Pietrzak E, Podwórny J (2016) Impulse excitation technique iet as a nondestructive method for determining changes during the gelcasting process. *Ceram Int* 42(3):3989. <https://doi.org/10.1016/j.ceramint.2015.11.067>
18. Raffmetal Datasheet en ab and ac 46100 - al si 11 cu 2 (fe). https://www.raffmetal.eu/web_ted/prodotti.asp?q=1 (2021). Accessed 5 Oct 2021
19. Oliver GMPWC (1992) An improved technique for determining hardness and elastic modulus using load and displacement sensing indentation. *J Mater Res* 7(6):1654
20. Lechner P, Filippov P, Kraschienski N, Ettemeyer F, Volk W (2020) A novel method for measuring elastic modulus of foundry silicate binders. *Int J Metalcasting* 14(2):423. <https://doi.org/10.1007/s40962-019-00361-w>
21. Dassault-Systems. Solid (continuum) elements. <https://abaqus-docs.mit.edu/2017/English/SIMACAEELMRefMap/simaelm-c-solidcont.htm>, lastaccessed2021-10-05 (2017). Accessed 5 Oct 2021

Publisher's Note Springer Nature remains neutral with regard to jurisdictional claims in published maps and institutional affiliations.